Research Article | Vol. 30, No. 17 / 15 Aug 2022 / Optics Express 31256
Optics EXPRESS

Near-eye display with a triple-channel waveguide for metaverse

CHAO PING CHEN,[1,*] YUEPENG CUI,[2] YE CHEN,[1] SHAN MENG,[1] YANG SUN,[1] CHAOJIE MAO,[2] AND QIANG CHU[1]

[1]*Smart Display Lab, Department of Electronic Engineering, Shanghai Jiao Tong University, Shanghai, China*
[2]*Shanghai InfoCrops Science & Technology Co., Ltd., Shanghai, China*
[*]*ccp@sjtu.edu.cn*

Abstract: We present a near-eye display featuring a triple-channel waveguide with chiral liquid crystal gratings. Our triple-channel waveguide is capable of dividing one field of view into three through both the polarization orthogonality and angular separation. To illustrate its principle, a *k*-space diagram, which takes into account the aspect ratio of field of view, is depicted. Our results demonstrate that its diagonal field of view reaches 90°, eye relief is 10 mm, exit pupil is 4.9×4.9 mm^2, transmittance is 4.9%, and uniformity is 89%.

© 2022 Optica Publishing Group under the terms of the Optica Open Access Publishing Agreement

1. Introduction

Lately, a buzzword called "metaverse" has been going viral across the globe. Despite being overhyped, metaverse is still in its infancy, lacking of mature technologies and products to deliver. For starters, one of the most crucial building blocks of metaverse is arguably the near-eye displays (NEDs), *e.g.* augmented/virtual reality (AR/VR) eyewear. The mainstream NEDs often come in three types of architectures, *i.e.* combiners [1–6], magnifiers [7–9], and waveguides [10–20]. Which type of architecture is ideal for NEDs? In the short run, combiners and magnifiers are prevailing in the sectors of AR and VR, respectively. However, in the long run, waveguides are tipped to overtake the former two for both AR and VR. This prediction is not groundless for several reasons. Number one, waveguides could support big field of views (FOVs). Number two, waveguides are compatible with minimal designs, more resembling normal eyeglasses. Number three, waveguides, by leveraging the total internal reflection (TIR), lend themselves to the exit pupil (EP) or eyebox expansion. Yet, waveguides have many issues too. One major concern, among others, is about the poor uniformity across the eyebox region. This is because that different fields propagate at different angles within the waveguide. And it will only get worse as the FOV becomes bigger. To address this issue, we hereby introduce a triple-channel-waveguide-based NED, which aims to push the FOV further without sacrificing the uniformity. In the subsequent sections, we will be discussing on how to design this type of architecture and exploring both its merits and limits.

2. Design rules

2.1. Triple-channel waveguide

Figure 1 shows a cross-section of our triple-channel waveguide, with its top, middle and bottom layers being referred to as channel 1, channel 2 and channel 3, respectively. The input FOV is divided equally into left (FOV_1), center (FOV_2) and right (FOV_3) sub-FOVs, which in turn carry the left-handed (L), right-handed (R) and left-handed circular polarizations. Accordingly, gratings—including the in-coupling and out-coupling—of channel 1/2/3 are responsive merely to $FOV_{1/2/3}$. This can be fulfilled by adjusting both the polarization selectivity and tilt angles $\theta_{1/2/3}$ of gratings. For the sake of big FOV, a lanthanum dense flint glass LASF35 (Schott) is chosen as

#470299 https://doi.org/10.1364/OE.470299
Journal © 2022 Received 13 Jul 2022; revised 31 Jul 2022; accepted 31 Jul 2022; published 11 Aug 2022

Optics EXPRESS

the material of waveguide, whose refractive index n_{wg} at 633/546/486 nm is 2.0149/2.0304/2.0471, yielding to a critical angle θ_c of 29.76°/29.51°/29.25°. To accommodate longer wavelengths, it would be safer to use a slightly larger angle, say 30°, as the common critical angle θ_c.

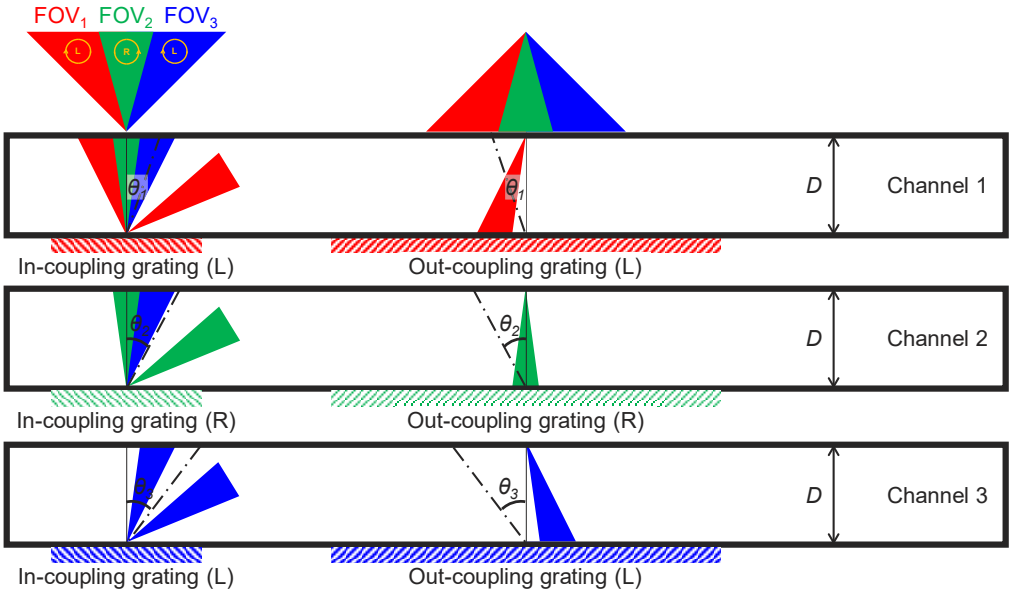

Fig. 1. Cross-section of triple-channel waveguide, with its top, middle and bottom layers being referred to as channel 1, channel 2 and channel 3, respectively. The input FOV is divided equally into left (FOV_1), center (FOV_2) and right (FOV_3) sub-FOVs, which in turn carry the left-handed (L), right-handed (R) and left-handed circular polarizations. Accordingly, gratings—including the in-coupling and out-coupling—of channel 1/2/3 are responsive merely to left/center/right sub-FOV.

2.2. *Upper limit of FOV*

Figure 2 plots the transition of FOV from air to waveguide in terms of wave vector space or k-space [19]. To avoid the excess notations, both abscissa and ordinate shall be divided by the free-space wavenumber k_0. Inside the innermost circle with a radius R_{air} lies the input FOV. Considering that the biggest rectangle inscribed in a circle is a square, we gravitate towards to equating the horizontal FOV (FOV_h) to the vertical FOV (FOV_v). The diagonal FOV—by default the one without subscript—can be correlated with the above two via

$$FOV = 2 \cdot tan^{-1}\left(\sqrt{tan^2\left(\frac{FOV_h}{2}\right) + tan^2\left(\frac{FOV_v}{2}\right)}\right) \tag{1}$$

Upon entering the waveguide, all three sub-FOVs will be located at the same region of k-space, meaning that the allowable field angles within each channel are identical. By invoking the invariance of k-space of FOV from air to waveguide [19], the radius R_{fov} of circumcircle of this region could be deduced as

$$R_{fov} = \sqrt{\left(n_{air} + 2n_{air}sin\left(\frac{FOV_h}{2}\right)\right)^2 + \left(n_{air}sin\left(\frac{FOV_v}{2}\right)\right)^2} \tag{2}$$

where n_{air} is the refractive index of air. When the circumcircle overlaps with the outermost circle—*i.e.* $R_{fov} = R_{wg}$—FOV reaches its maximum. While maintaining the aspect ratio of FOV

Optics EXPRESS

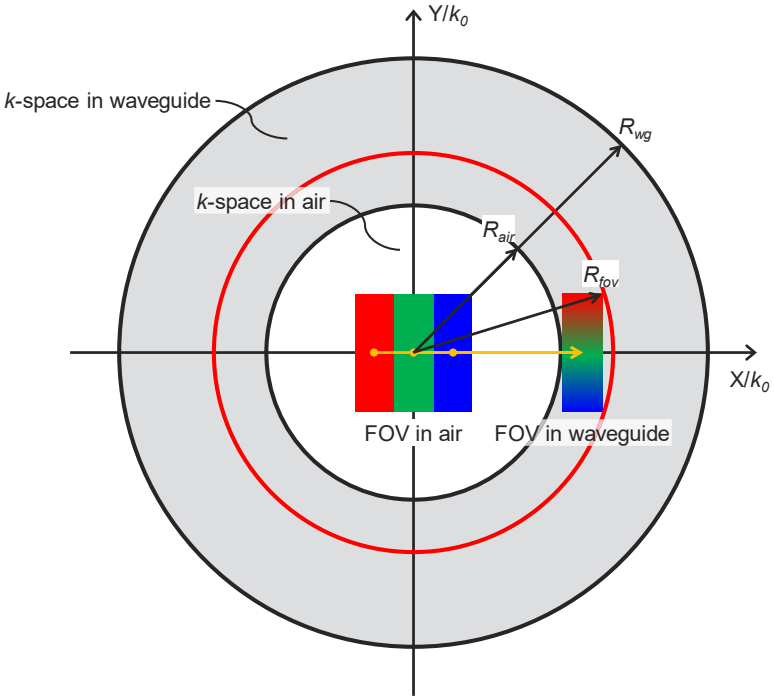

Fig. 2. *k*-space diagram of triple-channel waveguide. To avoid the excess notations, both abscissa and ordinate shall be divided by the free-space wavenumber k_0. Upon entering the waveguide, all three sub-FOVs will be located at the same region of *k*-space, meaning that the allowable field angles within each channel are identical.

as 1:1, the maximum diagonal FOV with respect to the refractive index of waveguide can be estimated, as shown in Fig. 3. Say $n_{wg} = 1.8$, the upper limits of FOVs are 60°/88°/121° for the single/dual/triple-channel waveguide, respectively. In our case, the input FOV is 90°, *i.e.* 70.4° (horizontal) × 70.4° (vertical). Then, FOV measured in the triple-channel waveguide is 11° (horizontal) × 33° (vertical).

2.3. Pupil duplication

Figure 4 illustrates how an input or entrance pupil with a diameter D_p—same as the length of in-coupling grating W_i—is duplicated through a succession of TIRs at an angle θ_{wg}. The number of pupils N is equivalent to the number of TIRs, which can be written as

$$N = \frac{W_o}{2Dtan\theta_{wg}} \tag{3}$$

where W_o is the length of out-coupling grating and D the thickness of waveguide. This equation is valid as long as θ_{wg} is greater than θ_c (30°). Otherwise, TIR will not occur. Given $W_o = 20$ mm and $D = 1.17$ mm, the number of pupils can be computed as a function of the angle of TIR, as shown in Fig. 5. As FOV_h in the waveguide is 11°, the angle of TIR θ_{wg} ranges from 30° to 41°, for which the number of pupils N is between 15 to 10.

Optics EXPRESS

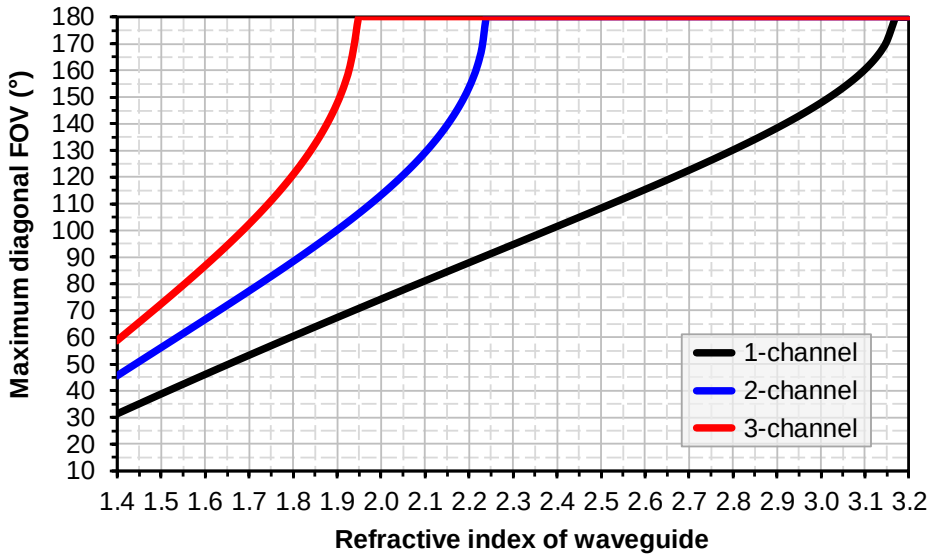

Fig. 3. Maximum diagonal FOV with respect to the refractive index of waveguide, while maintaining the aspect ratio of FOV as 1:1. Say $n_{wg} = 1.8$, the upper limits of FOVs are 60°/88°/121° for the single/dual/triple-channel waveguide, respectively.

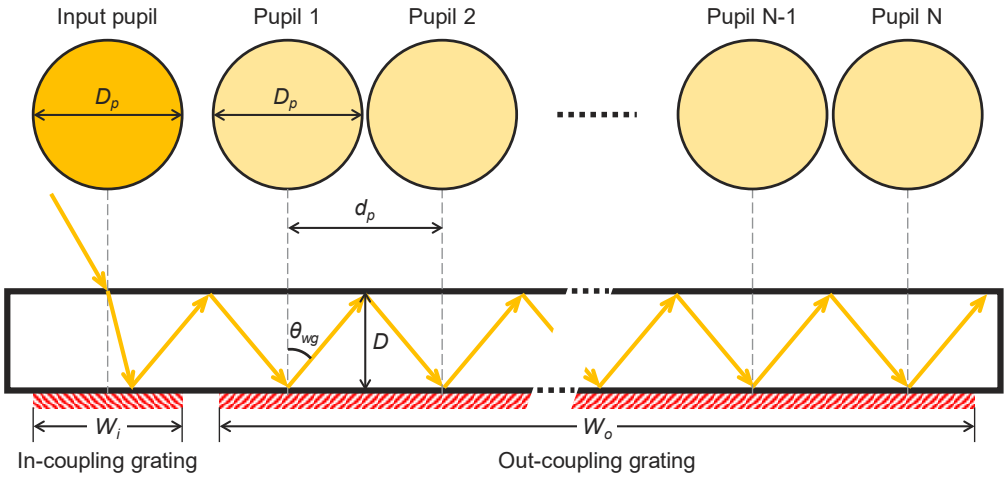

Fig. 4. Pupil duplication through a succession of TIRs at an angle θ_{wg}. The number of duplicated pupils N is equivalent to the number of TIRs.

Optics EXPRESS

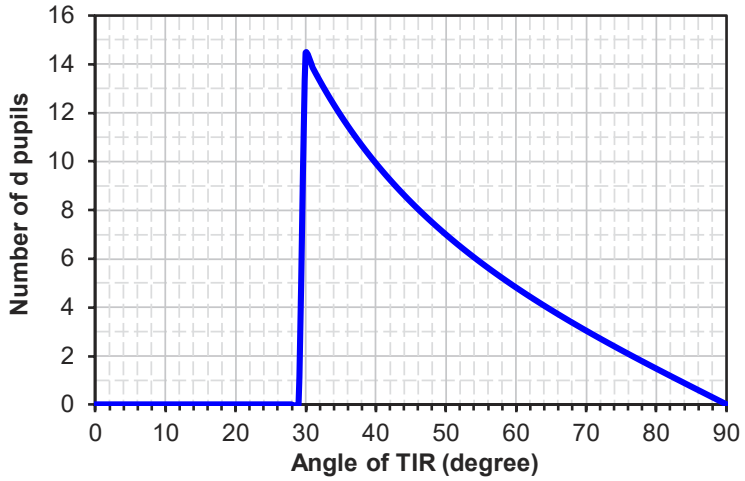

Fig. 5. Number of pupils computed as a function of the angle of total internal reflection when $W_o = 20$ mm and $D = 1.17$ mm. As FOV_h in the waveguide is 11°, the angle of TIR θ_{wg} ranges from 30° to 41°, for which the number of pupils N is between 15 to 10.

2.4. Intensity and uniformity

The uniformity measures the difference of irradiance or intensity across the pupils, which is defined as

$$Uniformity = \frac{2I_{min}}{I_{max} + I_{min}} \tag{4}$$

where I_{max} and I_{min} are the maximum and minimum intensities, respectively. When the interpupillary distance d_p is greater than D_p, there will be no overlap between the adjacent pupils. The intensity shall stay uniform among all pupils. When the interpupillary distance d_p is less than D_p, the adjacent pupils will overlap with one another. Suppose the out-coupling grating of each channel is composed of 10 sub-gratings. For a monochromatic light that is deemed as coherent, the intensity I of overlapped area above the mth sub-grating shall be given by [21]

$$I = I_0\eta_m + I_0(1-\eta_m)\eta_m + 2I_0\eta_m\sqrt{1-\eta_m}cos\left(\frac{4\pi n_{wg}D}{\lambda cos\theta_{wg}}\right) \tag{5}$$

where I_0 is the intensity of incident light, η_m the efficiency of mth sub-grating, and λ the wavelength. The above equations indicate that both the intensity and uniformity can be modulated by the grating efficiency. Combining Eq. (4) and Eq. (5), and letting $\lambda = 546$ nm, $\theta_{wg} = 35.5°$ (central field) and $D = 1.17$ mm, we could calculate the uniformity against the grating efficiency, as shown in Fig. 6. For grating efficiency varying from 0% to 100%, uniformity is between 83% and 100%, of which the average is 89%.

2.5. Chiral liquid crystal grating

As a viable option, we opt for chiral liquid crystal (CLC) [22] as both in-coupling and out-coupling gratings. To coordinate with the left/center/right $\text{FOV}_{1/2/3}$ switching, four things need to be checked for the gratings. First, the helix of CLC of channel 1/2/3—or CLC 1/2/3—must have the same handedness as that of circular polarization of $\text{FOV}_{1/2/3}$. Second, the tilt angle $\theta_{1/2/3}$ of

Optics EXPRESS

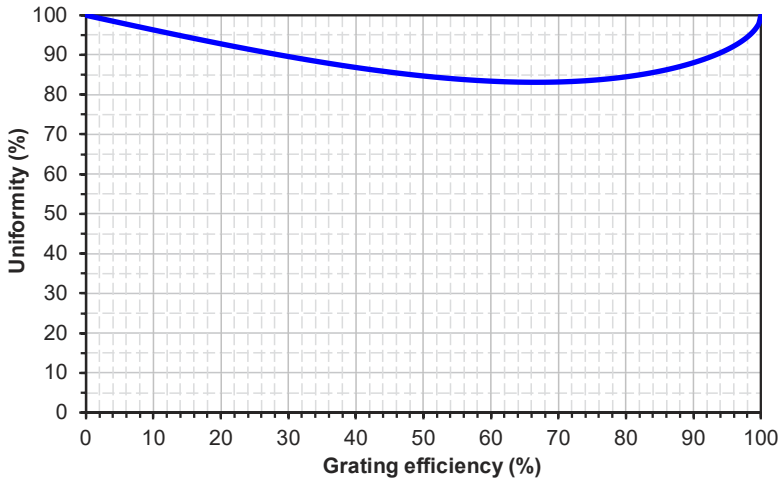

Fig. 6. Uniformity calculated against the grating efficiency. For grating efficiency varying from 0% to 100%, uniformity is between 83% and 100%, of which the average is 89%.

Table 1. Parameters of CLC gratings and ranges of field angles

Channel	Field (incident)	Field (refracted)	Field (reflected)	CLC grating	
1	−35.2° to −11.7°	−16.5° to −5.5°	30° to 41°	n_o	1.455
				n_e	1.545
				p	396 nm
				θ_1	12.25°
				θ_B	23.25°
2	−11.7° to 11.7°	−5.5° to 5.5°	30° to 41°	n_o	1.455
				n_e	1.545
				p	382 nm
				θ_2	17.75°
				θ_B	17.75°
3	11.7° to 35.2°	5.5° to 16.5°	30° to 41°	n_o	1.455
				n_e	1.545
				p	372 nm
				θ_3	23.25°
				θ_B	12.25°

Optics EXPRESS

CLC gratings should meet

$$\theta_{1/2/3} = \frac{\theta_c + \theta_R}{2} \tag{6}$$

where θ_R stands for the rightmost field angle of $FOV_{1/2/3}$. This condition guarantees that left edge of $FOV_{1/2/3}$ in waveguide—whose orientation is opposite to that of $FOV_{1/2/3}$ in air due to the reflective in-coupling—adjoins the innermost circle of k-space. Third, as the CLCs of channel 1 and channel 3 are of the same handedness, it is important to separate their Bragg angles θ_B so as to keep the light of FOV_3 from being reflected by the in-coupling grating of channel 1. If not to alter the host material of CLCs for each channel, θ_B can be modified by tuning the helical pitch p as [23]

$$cos\theta_B = \frac{2\lambda}{p(n_o + n_e)} \tag{7}$$

where n_o/n_e is the ordinary/extraordinary refractive index of liquid crystal (LC). Fourth, the refractive anisotropy or birefringence Δn and/or thickness of LC shall be big enough such that the angular bandwidth of CLC becomes comparable to $FOV_{1/2/3}$ [24]. Putting everything together, Table 1 summarizes the parameters of CLC gratings and ranges of field angles, which are incident from air, refracted by waveguide, and reflected by CLC, respectively.

3. Results and discussion

3.1. Grating efficiency

We adopt the Berreman 4×4-matrix method [25] and the parameters given in Table 1 for the quantitative analysis of CLCs. Figure 7 is a graph of the normalized efficiency of CLC 1/2/3 versus the grating thickness. Despite their Bragg angles being different, efficiencies of all CLCs coincide with each other. When the thickness exceeds 6 μm, the efficiency will max out at 100%. As for the angular bandwidth, normalized efficiency of CLC 1/2/3 with a thickness of 5 μm is plotted against the incident angle—measured relative to the grating normal—as shown in Fig. 8. Over the entire range of field angles of $FOV_{1/2/3}$, the average efficiency of CLC 1/2/3 is 87%, 94% and 97%, respectively. Of all angular ranges, the small-angle regime (0° to 6.75°) of CLC 1 merits special care in that FOV_3—partially reflected by CLC 1 prior to arriving at CLC 3—will face a mild loss (< 3.4%).

3.2. Waveguide simulation

To simulate the waveguide, we resort to the light guide toolbox of VirtualLab Fusion. Since the FOV is equally divided and all angles propagating within channel 1/2/3 are identical, channel 2, where the center of FOV or FOV_2 is located, is selected. The optical setup for our simulation is shown in Fig. 9, where the sub-gratings of out-coupling grating are labeled as O1 to O10. The thickness D of waveguide is 1.17 mm. The width W_i of in-coupling grating shall match with the size of input pupil—a circle with a diameter D_p of 2 mm. The width W_o of out-coupling grating is 20 mm, with each sub-grating being 2 mm across. Hence, if the eye relief is 10 mm, exit pupil will be 4.9×4.9 mm^2. The input intensity I_0 of the source is normalized to be 1 V^2/m^2. From the ray tracing, the footprints of duplicated pupils of central field can be obtained, as shown in Fig. 10. On top of the footprints, Fourier modal method [26] is employed to calculate the electromagnetic fields captured by the detector. For the fields of overlapped regions, the coherent summations are applied. After the optimization, the normalized grating efficiencies of reflected zeroth (R0) and first (R1) orders are tweaked as in Table 2. As I_{min}= 0.0433 V^2/m^2 and I_{max}= 0.0541 V^2/m^2, the transmittance—the ratio of (I_{min}+I_{max})/2 to I_0—and uniformity are 4.9% and 89%, respectively.

Optics EXPRESS

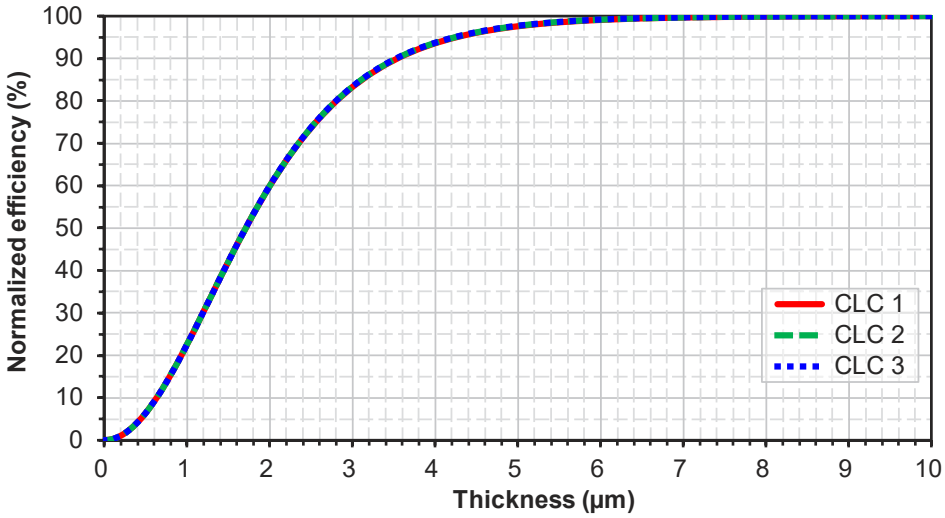

Fig. 7. Normalized efficiency of CLC 1/2/3 versus the grating thickness. When the thickness exceeds 6 μm, the efficiency will max out at 100%.

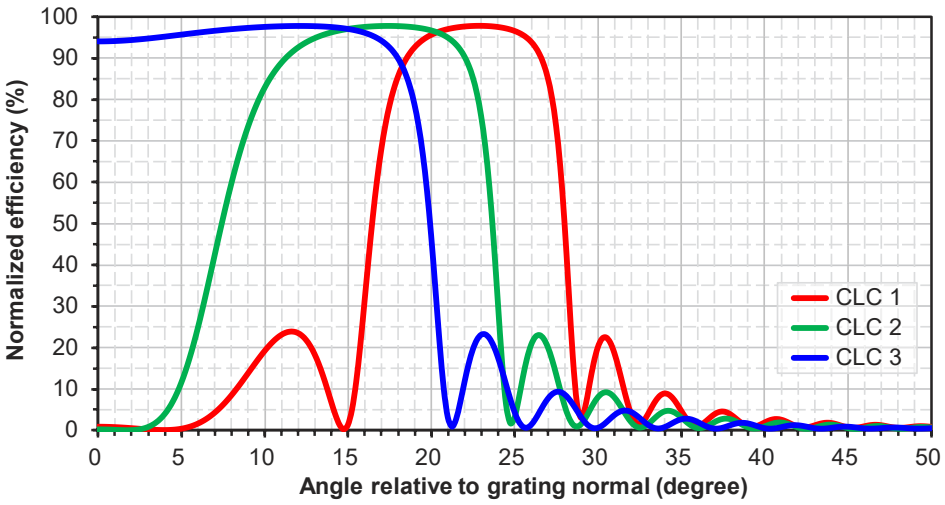

Fig. 8. Normalized efficiency of CLC 1/2/3 with a thickness of 5 μm against the angle relative to grating normal. Over the entire range of field angles of $FOV_{1/2/3}$, the average efficiency of CLC 1/2/3 is 87%, 94% and 97%, respectively.

Optics EXPRESS

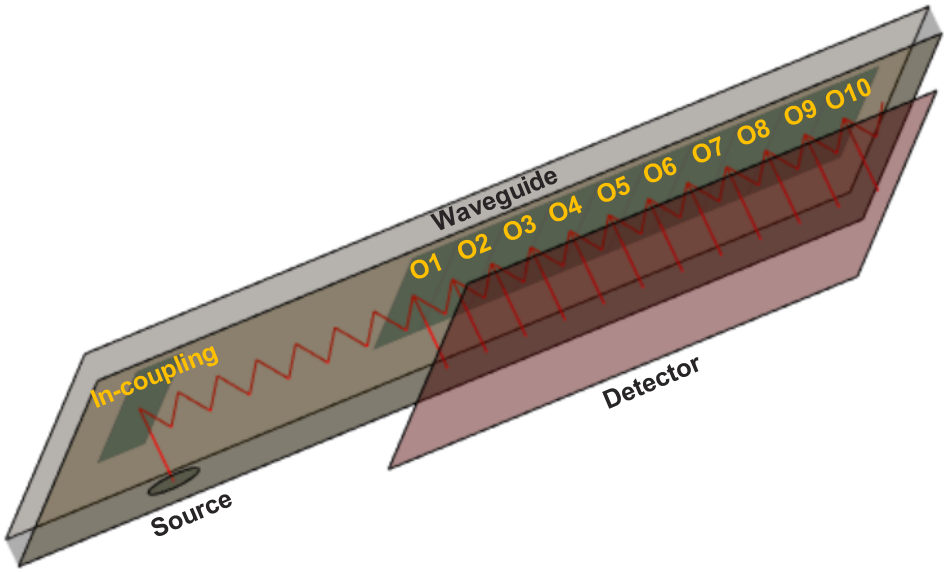

Fig. 9. Optical setup for the simulation on VirtualLab Fusion. The sub-gratings of out-coupling grating are labeled as O1 to O10. The thickness D of waveguide is 1.17 mm. The width W_i of in-coupling grating shall match with the size of input pupil—a circle with a diameter D_p of 2 mm. The width W_o of out-coupling grating is 20 mm, with each sub-grating being 2 mm across.

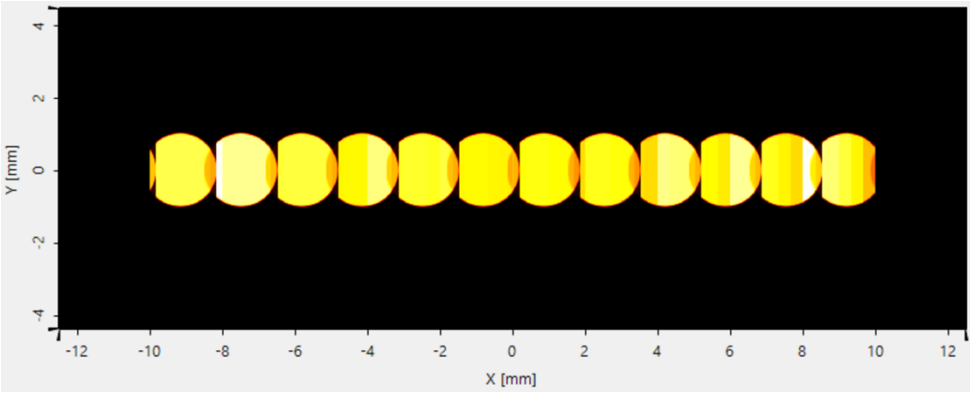

Fig. 10. Footprints and intensities of duplicated pupils of central field. For the fields of overlapped regions, the coherent summations are applied. As I_{min}= 0.0433 V^2/m^2 and I_{max}= 0.0541 V^2/m^2, the transmittance and uniformity are 4.9% and 89%, respectively.

Optics EXPRESS

Table 2. Normalized efficiencies of gratings

Grating	Efficiency of R0 (%)	Efficiency of R1 (%)
In-coupling[a]	6	94
O1	89.8	10.2
O2	90.9	9.1
O3	90.9	9.1
O4	89.2	10.8
O5	88.7	11.3
O6	86.8	13.2
O7	84.6	15.4
O8	79.2.	20.8
O9	72.61	27.39
O10	57.7	42.3

[a]Efficiency of in-coupling grating is consistent with the average efficiency of CLC 2.

4. Conclusions

In a nutshell, a NED with a triple-channel waveguide has been proposed. Several key performance indicators have been numerically evaluated. FOV is 90° (diagonal), eye relief is 10 mm, exit pupil is 4.9×4.9 mm^2, transmittance is 4.9%, and uniformity is 89%. Three major contributions are identified as follows. Contribution 1. FOV wise, the triple-channel waveguide beats out its closet variants, *e.g.* the dual-channel waveguides [13,19,20] or the alike [15,17]. Contribution 2. Compared to the other works [15,19], our derivation of upper limit of FOV is more accurate by factoring into the aspect ratio of FOV. Contribution 3. How the grating efficiency modulates the uniformity is formulated. This would enable the designers to roughly estimate the uniformity from scratch. Those being said, this type of NED is far from being perfect. Among other things, the angular separation of sub-FOVs of channel 1 and channel 3 is incomplete. Also, no doubt, the additional channel of waveguide will translate into an increase in both the complexity and cost.

Funding. National Natural Science Foundation of China (61901264, 61831015); Science and Technology Commission of Shanghai Municipality (19ZR1427200); Natural Science Foundation of Chongqing (cstc2021jcyj-msxmX1136).

Acknowledgments. Special thanks to LightTrans International GmbH in Germany for offering the official license of VirtualLab Fusion.

Disclosures. The authors declare no conflicts of interest.

Data availability. Data underlying the results presented in this paper are not publicly available at this time but may be obtained from the authors upon reasonable request.

References

1. J. P. Rolland, "Wide-angle, off-axis, see-through head-mounted display," Opt. Eng. **39**(7), 1760–1767 (2000).
2. L. Zhou, C. P. Chen, Y. Wu, Z. Zhang, K. Wang, B. Yu, and Y. Li, "See-through near-eye displays enabling vision correction," Opt. Express **25**(3), 2130–2142 (2017).
3. C. Hong, S. Colburn, and A. Majumdar, "Flat metaform near-eye visor," Appl. Opt. **56**(31), 8822–8827 (2017).
4. G.-Y. Lee, J.-Y. Hong, S. Hwang, S. Moon, H. Kang, S. Jeon, H. Kim, J.-H. Jeong, and B. Lee, "Metasurface eyepiece for augmented reality," Nat. Commun. **9**(1), 4562 (2018).
5. L. Mi, C. P. Chen, Y. Lu, W. Zhang, J. Chen, and N. Maitlo, "Design of lensless retinal scanning display with diffractive optical element," Opt. Express **27**(15), 20493–20507 (2019).
6. B. C. Kress, *Optical Architectures for Augmented-, Virtual-, and Mixed-Reality Headsets* (SPIE, 2020).
7. J. E. Melzer and K. Moffitt, *Head-Mounted Displays: Designing for the User* (McGraw-Hill, 1997).
8. W. Barfield, *Fundamentals of Wearable Computers and Augmented Reality* (2nd ed.) (CRC, 2016).
9. J. Xiong, E.-L. Hsiang, Z. He, T. Zhan, and S.-T. Wu, "Augmented reality and virtual reality displays: emerging technologies and future perspectives," Light: Sci. Appl. **10**(1), 216 (2021).

Optics EXPRESS

10. Y. Amitai, "Extremely compact high-performance HMDs based on substrate-guided optical element," in *SID Symposium Digest of Technical Papers* (2004), pp. 310–313.
11. T. Levola, "Diffractive optics for virtual reality displays," J. Soc. Inf. Disp. **14**(5), 467–475 (2006).
12. H. Mukawa, K. Akutsu, I. Matsumura, S. Nakano, T. Yoshida, M. Kuwahara, and K. Aiki, "A full-color eyewear display using planar waveguides with reflection volume holograms," J. Soc. Inf. Disp. **17**(3), 185–193 (2009).
13. T. Vallius and J. Tervo, "Waveguides with extended field of view," US Patent 9,791,703 B1 (2016).
14. Y. Wu, C. P. Chen, L. Zhou, Y. Li, B. Yu, and H. Jin, "Design of see-through near-eye display for presbyopia," Opt. Express **25**(8), 8937–8949 (2017).
15. Z. Shi, W. T. Chen, and F. Capasso, "Wide field-of-view waveguide displays enabled by polarization-dependent metagratings," Proc. SPIE **10676**, 1067615 (2018).
16. D. Grey and S. Talukdar, "Exit pupil expanding diffractive optical waveguiding device," US Patent 10,359,635 B2 (2018).
17. C. Yoo, K. Bang, M. Chae, and B. Lee, "Extended-viewing-angle waveguide near-eye display with a polarization-dependent steering combiner," Opt. Lett. **45**(10), 2870–2873 (2020).
18. W. Zhang, C. P. Chen, H. Ding, L. Mi, J. Chen, Y. Liu, and C. Zhu, "See-through near-eye display with built-in prescription and two-dimensional exit pupil expansion," Appl. Sci. **10**(11), 3901 (2020).
19. C. P. Chen, L. Mi, W. Zhang, J. Ye, and G. Li, "Waveguide-based near-eye display with dual-channel exit pupil expander," Displays **67**, 101998 (2021).
20. C. P. Chen, L. Mi, W. Zhang, J. Ye, and G. Li, "Wide-field-of-view near-eye display with dual-channel waveguide," Photonics **8**(12), 557 (2021).
21. F. L. Pedrotti, L. M. Pedrotti, and L. S. Pedrotti, *Introduction to Optics* (3rd ed.) (Cambridge University Press, 2017), Chap. 7.
22. J. Cao, C. P. Chen, B. S. Bae, J.-K. Song, D. S. Kim, and C. G. Jhun, "Enhanced reflectance of cholesteric liquid crystal device with quantum dots," Mol. Cryst. Liq. Cryst. **613**(1), 59–62 (2015).
23. D.-K. Yang and S.-T. Wu, *Fundamentals of Liquid Crystal Devices* (2nd ed.) (Wiley, 2014).
24. B. S. Bae, S. Han, S. S. Shin, K. Chen, C. P. Chen, Y. Su, and C. G. Jhun, "Dual structure of cholesteric liquid crystal device for high reflectance," Electron. Mater. Lett. **9**(6), 735–740 (2013).
25. D. W. Berreman, "Optics in stratified and anisotropic media: 4×4-matrix formulation," J. Opt. Soc. Am. **62**(4), 502–510 (1972).
26. L. Li, "New formulation of the Fourier modal method for crossed surface-relief gratings," J. Opt. Soc. Am. A **14**(10), 2758–2767 (1997).

101.224.227.54 {ts '2022-08-12 10:41:47'}